Optical Characterization of the Director Field in a Distorted Nematic Layer

Emmanuel Plaut, Alain Joets, Roland Ribotta

Optical Characterization of the Director Field in a Distorted Nematic Layer

Emmanuel Plaut, Alain Joets (*) and Roland Ribotta

Laboratoire de Physique des Solides, Université Paris-Sud, 91405 Orsay Cedex, France

(Received 30 June 1997, accepted 22 August 1997)

PACS.78.20.Bh – Theory, models, and numerical simulation
PACS 42 70.Df – Liquid crystals
PACS.47.20.Bp – Buoyancy-driven instability

Abstract. — We develop new optical methods using transmitted polarized light for the characterization of the out of plane component n_z of the director field in a weakly distorted planar nematic layer. In extraordinary light, we relate the angles of aperture of the caustic surface to the local amplitudes of the n_z distortion. In ordinary light, a new type of contrast due to the anisotropic light scattering is shown to give the map of n_z^2. We apply our methods to the study of the director distortions occuring in the thermal convection.

1. Introduction

Among the methods used in experimental physics for the characterization of continuous media, the *optical* ones have the important advantage of being non-perturbative. For instance, in hydro- or aero-dynamics, the shadowgraph method can give access rather directly to the gradients of the refractive index, and thus to some local fields of the fluids such as the density or the temperature field [1]. The interpretation of the images is usually made under the assumption of small deviations of the rays. This restriction breaks down in several cases, for instance in nematohydrodynamics because of the high birefringence of nematic liquid crystals. In this article, we develop new optical methods for the local or global characterization of the director field in a uniaxial nematic layer. These methods might be applied to a wide class of director distortions, for instance those obtained in the study of the transition to spatio-temporal complexity in liquid crystals [2].

The optical axis in uniaxial nematic liquid crystals is the director field **n**, the average orientation of the rod shaped molecules. One distinguishes *extraordinary light*, where the electric field has a component along **n**, from *ordinary light*, where the electric field is perpendicular to **n**.

In extraordinary light, the ray index depends on the angle between the Poynting vector and **n**: this leads in general to a spectacular focusing of the rays onto caustics, and it explains why this light is most commonly used for the geometrical characterization of the director field (spatial periodicity, *etc.*). Also, some measurements of the heigth of focusing of the caustic

(*) Author for correspondence (e-mail joets@lps.u-psud fr)

cusps have been used to extract the amplitude of the director distortion [3]. The accuracy of these measurements is however poor, since because of the nonzero value of the wavelength, the caustics appear to have a finite thickness, which is particularly large at the cusp points. We will show in section 2 that the amplitude of the director distortion can be extracted more easily from the measure of aperture angles of the caustics.

In ordinary light, the index is independent of the director field, so usually weaker effects are obtained as compared with extraordinary light. For this reason, the ordinary light was seldom used in nematodynamics studies. We will show in section 3 that, in thick nematic layers, interesting anisotropic scattering effects lead to a contrast explicitly function of the angle of the bend distortion averaged over the layer.

Our methods will be illustrated in the case of the *thermoconvection of an horizontally extended planar nematic layer*, where the director is set to an horizontal direction $\hat{\mathbf{x}}$ at the horizontal boundary plates, and thus in the bulk $\mathbf{n} = \hat{\mathbf{x}}$ at rest. A light beam of parallel rays is sent through the layer from below (along the vertical direction $\hat{\mathbf{z}}$). The extraordinary light is selected by a polarizer parallel to $\hat{\mathbf{x}}$, and the ordinary light by a polarizer perpendicular to $\hat{\mathbf{x}}$, *i.e.* parallel to $\hat{\mathbf{y}}$. Distortions of the director field are obtained by heating from below, when the applied vertical thermal gradient ΔT exceeds a threshold value ΔT_c [4]. In our cells, of typical thickness $d = 1.3$ mm, $\Delta T_c \simeq 1$ °C. Near threshold, one obtains the normal rolls, of wavevector $\mathbf{q} = q\hat{\mathbf{x}}$, *i.e.* of axis normal to the anchoring direction $\hat{\mathbf{x}}$. When the reduced control parameter $\epsilon = \Delta T/\Delta T_c - 1$ is increased (nonlinear regime), the global symmetry of the system $\hat{\mathbf{y}} \mapsto -\hat{\mathbf{y}}$ breaks down, and the system bifurcates towards oblique rolls, of wavevector $\mathbf{q} = q\hat{\mathbf{x}} + p\hat{\mathbf{y}}$ with $p \neq 0$ [5]. Further increasing ϵ leads finally to a varicose structure [5], that we will more particularly study in Section 3.3. Our experimental results are obtained at zero or very weak director-stabilizing magnetic field $\mathbf{H} = H\hat{\mathbf{x}}$ ($H \lesssim 3H_F$ where H_F is the characteristic splay Fréederickz field). We use the nematic liquid crystal 5CB for which all material parameters are known. We study hereafter the regime of the "weak distortions": at not too high values of ϵ ($\epsilon \lesssim 0.7$), the director field appears to vary continuously on a characteristic scale of the order of the cell thickness. More precisely, we will use in model calculations the following simple form for the distortion of the vertical component of the director (which turns out to play the leading role, see below):

$$n_z(\mathbf{r}, z) = \tilde{n}_z(\mathbf{r}) \sin(\pi z). \tag{1}$$

There we note $\mathbf{r} = x\hat{\mathbf{x}} + y\hat{\mathbf{y}}$ the horizontal position in the layer, and z the vertical coordinate. The lengths are scaled in units of the layer thickness d; $z = 0$ (resp. 1) is the lower (resp. upper) plane of the layer. The form (1) can be justified theoretically in the weakly nonlinear regime $\epsilon \ll 1$ [6,7]. As we will see, (1) allows a good reconstruction of all the optical properties of the structures in the weak distortion regime, and it appears therefore to be a good approximation of the n_z field in this regime.

2. Extraordinary Light: the Caustics

2.1. PROPAGATION OF THE RAYS. — In a extraordinary light wave, the direction of propagation of the energy, *i.e.* of the ray, pointed by the Poynting vector $\mathbf{P}$, differs generally from the direction of propagation of the phase, pointed by the wavevector $\mathbf{k}$. Consequently the energy velocity differs from the phase velocity, and two different optical indices must be introduced [8]: the ray index n_r associated with the energy velocity, and the phase index n_p associated with the phase velocity. The ray index depends on the angle $\theta_r = (\widehat{\mathbf{n}, \mathbf{P}})$ according to:

$$n_r^2 = n_o^2 \cos^2 \theta_r + n_e^2 \sin^2 \theta_r \tag{2}$$

where n_o is the ordinary index and n_e is the extraordinary index [8,9]. For the nematic liquid crystal 5CB at a mean temperature of 28 °C used in our experiments, $n_e = 1.689$, $n_o = 1.536$, and thus the birefringence $\Delta n = n_e - n_o = 0.153$ [10]. The phase index depends on the angle $\theta_p = (\widehat{\mathbf{n}, \mathbf{k}})$ [8]:

$$\frac{1}{n_p^2} = \frac{\cos^2 \theta_p}{n_o^2} + \frac{\sin^2 \theta_p}{n_e^2} \tag{3}$$

θ_p differs from θ_r by the angle $\delta = (\widehat{\mathbf{P}, \mathbf{k}})$:

$$\delta = \theta_p - \theta_r = \theta_p - \arctan(\frac{n_o^2}{n_e^2} \tan \theta_p). \tag{4}$$

The Fermat principle still applies in anisotropic media, and it expresses that the extraordinary rays propagate in order to minimize the optical path $\int n_r \, ds$ [11]. The variation of n_r (2) due to the director distortion, *i.e.* to the variations of θ_r, is Δn: it represents here 10% of the index value. On the other hand, in thermoconvection, the temperature dependence of the indices [10]:

$$\frac{dn_e}{dT} = -0.0023 \text{ K}^{-1}, \quad \frac{dn_o}{dT} = 0.0005 \text{ K}^{-1}$$

induces, for a typical temperature variation of 1 °C, variations of n_r of less than 0.1%. The director induced index variations are much larger than the temperature induced index variations, and thus n_o and n_e can be taken as constant in (2).

In the propagation of an extraordinary ray inside the nematic layer, the direction of $\mathbf{P}$ tangent to the ray stays close to its initial value $\hat{\mathbf{z}}$, and thus the angle $\theta_r = (\widehat{\mathbf{n}, \mathbf{P}})$ is quasi insensitive to any horizontal rotation of the director, as we checked it in our calculations. This implies that, of the two components of $\mathbf{n}$, n_y and n_z (they give n_x through the geometric condition $\mathbf{n}^2 = 1$), n_z controls the deviation of the rays, whereas n_y can be taken equal to zero. In the case of the roll convective structures obtained in convection experiments near threshold, the n_z distortion is given by (1) with:

$$\tilde{n}_z(\mathbf{r}) = N_z \sin(\mathbf{q} \cdot \mathbf{r}) \tag{5}$$

where $\mathbf{q} = q\hat{\mathbf{x}} + p\hat{\mathbf{y}}$ is the wavevector of the rolls. From (2) and (1), (5) we write the Euler-Lagrange equations associated with the Fermat principle. They are solved numerically by the Runge-Kutta method of order 4. The caustic points are then deduced from the emerging set of straight rays by using the general method of [13].

2.2. GEOMETRY OF THE CAUSTIC. — The axis of the rolls is a direction of translational invariance, and consequently one has only to study the intersection of the caustic with the plane $(\mathbf{q}, \hat{\mathbf{z}})$. This intersection is composed of pairs of *fold* lines with opposite curvature which meet at *cusp* points: see Figure 1, which presents typical results of our calculations, for rolls with $\mathbf{q} = \pi\hat{\mathbf{x}}$ (the rolls are generally square-shaped, *i.e.* of period 2 in units of d) . The cusps are located above the separation planes between two adjacent rolls, *i.e.* above the up or down flows which are respectively the warm and cold flows in thermoconvection. In the experiments, the liquid crystal is confined between glass plates. The thermal regulation is insured by a layer of circulating water along those plates, and finally another glass plate is superimposed on top of the convection cell. This layered structure complicates the calculation of the height of the cusps: this focusing can occur inside any of the top layers depending on the amplitude of the distortion, and one has then to take into account the index and the thickness of the various layers. On the contrary, the two local maxima α_1 and α_2 of the deflection angle $i(x)$

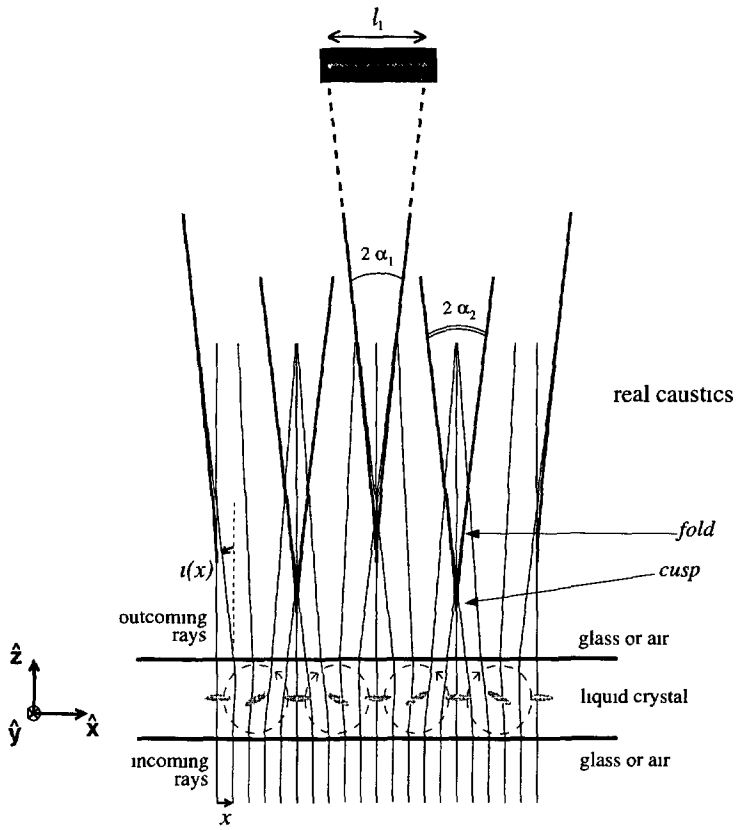

Fig 1. — Real caustics associated with a normal roll distortion given by equation (5), with $\mathbf{q} = \pi\hat{\mathbf{x}}$ and $N_z = \sin 40°$. The virtual caustics, envelope of the continuation of the outcoming rays and located below the layer, are not shown. The director distortion is sketched by the rod-like "molecules" in the mid-plane of the layer, and the corresponding flow by the dashed lines with arrows. The three cusps shown are associated respectively to up-flow, down-flow, up-flow edges In the experiments, the nematic layer is sandwiched between glass plates, but for the computation of the half angles α_1 and α_2 of aperture of the cusps, we can assume that air directly surrounds the nematic (see text). The angles α_i are measured experimentally by intercepting the cusp at a distance h from the top of the cell with a screen One then observes a bright band (picture shown in insert), the length of which can easily be measured.

measured in the air (Fig. 1) do not depend on the top layers of the experimental setup because of the transitivity of the laws of refraction. The angles α_i can thus be calculated assuming that air immediately surrounds the nematic, *i.e.* just taking into account the refraction at one dioptre nematic/air. Moreover, these angles, associated with the asymptotical branches of the caustics, appear as the half-angles of aperture of the cusps in the air, which can be easily measured experimentally.

We have numerically computed the angles α_i as a function of the amplitude N_z of the n_z distortion (5) for $\mathbf{q} = \pi\hat{\mathbf{x}}$. We have found the following scaling law:

$$\alpha_1 = 13.8\, N_z^2, \quad \alpha_2 = 15.6\, N_z^2 \tag{6}$$

with the angles α_i in degrees (Fig. 2). This leads to a *measurement of the amplitude* N_z

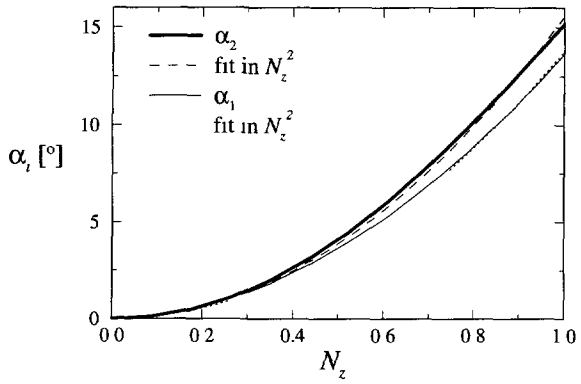

Fig 2 — Numerically computed values of the half-angles α_i of aperture of the cusps (see text), as a function of the amplitude N_z of the n_z distortion (5) with $\mathbf{q} = q\hat{\mathbf{x}}$. Fits of the angles α_i in N_z^2 give very good results.

according to the very simple formulae:

$$N_z = 0.269\sqrt{\alpha_1}, \quad N_z = 0.254\sqrt{\alpha_2} \tag{7}$$

These relations are also valid in the case of oblique rolls structures, at least for not too large p values. We computed as a test the values of $\alpha_i(N_z)$ for $q = \pi$, $p = q \tan 10^o$, and, in addition to the n_z distortion, a n_y distortion given by $n_y(\mathbf{r}, z) = 0.5 \sin(\pi z)$, which has been predicted to develop in oblique rolls by the weakly nonlinear model [7]. The relations (6), (7) still hold in this case, with coefficients that have varied of less than 1%. On the other hand, the coefficients in (6), (7) depend on the modulus $|\mathbf{q}|$ of the wavevector. In the domain $2.80 < |\mathbf{q}| < 3.50$, $|\arctan(p/q)| < 10^o$, where the wavevector of the rolls is found experimentally, we calculated the following relationship:

$$\frac{N_z}{\sqrt{\alpha_1}} = 0.269 - 0.040\ (|\mathbf{q}| - \pi), \quad \frac{N_z}{\sqrt{\alpha_2}} = 0.254 - 0.044\ (|\mathbf{q}| - \pi). \tag{8}$$

It shows that, for the same N_z values, the angles α_i increase with $|\mathbf{q}|$, since then the gradients of the director increase. However, the amplitude of the variations of the coefficients (8) is of less than $\pm 6\%$ in the domain $2.80 < |\mathbf{q}| < 3.50$, so in the following we will only use (7) for the estimation of the accuracy of our method.

Experimentally, the large value of the rolls diameter allows us to use a small laser beam to form, by illumination from below, just one cusp and the associated cone. We intercept this cone on a screen located at a distance h of the upper boundary of the cell, and obtain a bright band (Fig. 1) of length l_i along $\hat{\mathbf{x}}$ ($i = 1$ for down-flow cusps, 2 for up-flow cusps). Assuming that the cusp point is located right at the upper boundary of the cell, we obtain $\alpha_i = D^{-1} \arctan(l_i/(2h))$ (with $D = \pi/180$ to have α_i in degrees). In fact, the height h_c of the cusp point is given, for not too large N_z values, by [14]:

$$h_c \simeq \frac{0.5\, d}{N_z^2}$$

An interesting aspect of our method is that the experimental error on the real value of h, $\delta h \simeq h_c$, is in fact negligible because of the small values of α_i at small N_z. Indeed, the error

on α_i is given by:

$$\delta\alpha_i \simeq D^{-1}\frac{1}{1+\tan^2(D\alpha_i)}[\frac{\delta l_i}{2h}+\tan(D\alpha_i)\frac{\delta h}{h}]$$

where the factor $\tan(D\alpha_i) \sim N_z^2$ will balance the divergence of $\delta h \sim h_c \sim N_z^{-2}$. We estimate, with our experimental values $d = 1.52$ mm, $h = 273$ mm, $\delta l_i = 1$ mm, that the error on α_i is always less than 0.15°. Since α_1 is the smallest angle, *i.e.* the one which produces the largest error on N_z, we then deduce from (7):

$$\delta N_z \simeq \frac{0.02}{\sqrt{\alpha_1}} \simeq \frac{0.005}{N_z}.$$

Therefore this method is inadequate for the measurement of small amplitudes which lead to extremely small cusp angles. The smallest measurable amplitude, with an accuracy of 10% (*i.e.* $\delta N_z/N_z < 0.1$), is of the order of $N_z = 0.2 = \sin 12^o$.

Our numerical results imply that, independently of the amplitude of the distortion, the ratio α_2/α_1 should be constant. As a first test of the method we computed from our experimental measurements and for not too small N_z, the mean value and the standard deviation of this ratio ([1]). We obtained:

$$<\frac{\alpha_2}{\alpha_1}>= 1.14\,,\quad <(\frac{\alpha_2}{\alpha_1})^2>-<\frac{\alpha_2}{\alpha_1}>^2>^{1/2}= 0.02$$

in excellent agreement with our theoretical predictions, which give $\alpha_2/\alpha_1 = 1.13 \pm 0.015$ (depending on $|\mathbf{q}|$, see (8)). It must be noted that our measurements were performed in various conditions, on normal and oblique roll structures, at various magnetic fields. The extremal values that we measured for α_2/α_1 (with a relative error < 15%) are 1.09 and 1.21.

2.3. APPLICATIONS. — By this method we could determine for the first time, from the measurements of the amplitude, the characteristic time T_0 of the thermoconvective instability, and thus we could check the linear model developped for this instability [4, 6]. After applying a step of the thermal gradient from above to slightly below threshold, the decrease of all convective amplitudes is governed by the linear evolution operator which, for distortions close to the critical one (the one which develops spontaneously just above threshold), reduces to:

$$\partial_t N_z = \sigma N_z \quad \Rightarrow \quad N_z(t) = N_z(0)\, e^{\sigma t}$$

where σ is the growth rate of the bifurcated amplitude. For small values of the reduced control parameter ϵ, the growth rate should be $\sigma = T_0^{-1}\epsilon$. Figure 3a shows a typical sequence of N_z measurements performed after a step to below threshold. During the experiment $\mathbf{q}$ (needed in (8)) does not vary, and is measured once using a numerical Fourier transform of the initial roll pattern. The amplitude is found to follow closely the expected exponential decaying law, as it is confirmed by the comparison with exponential fits. These fits give the growth rate σ, and T_0 is estimated as ϵ_f/σ, where $\epsilon_f < 0$ is the final value of ϵ As a function of the secondary parameter H which is the stabilizing magnetic field along x, measured in units of a characteristic Fréedericksz field as in [6], we obtain finally for $T_0(H)$ a good agreement with the predictions of the linear model [6], as shown in Figure 3b. Our method is well adapted to the study of roll structures with rather high N_z amplitudes, and we will present in a forthcoming paper a study of the nonlinear saturation, *i.e.* the law $N_z(\epsilon)$, by this method.

([1]) For small N_z, the relative error on α_2/α_1, which we estimated as $0.4/\alpha_1 \simeq 0.03/N_z^2$, diverges. We only retained the measurement where this error was smaller than 15%.

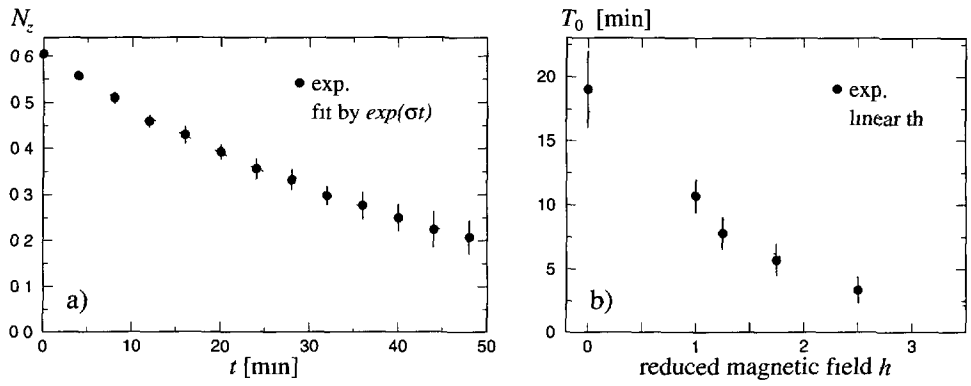

Fig. 3. — a) The convection amplitude N_z after a step from $\epsilon_i = 0.06$ to $\epsilon_f = -0.17$. The stabilizing magnetic field is $H = 1.25$ in units of the characteristic Fréedericksz field (see text). Note that the errorbars increase when N_z becomes too small. The fit shows that the decaying law is in $\exp(\sigma t)$, with $\sigma = -0.0223$ min^{-1}, from which one obtains $T_0 = 7.62$ min b) deduced values of the characteristic time T_0, as a function of the stabilizing magnetic field. They are in good agreement with the predictions of the linear model (dotted line).

3. Ordinary Light: Anisotropic Scattering

For other convective structures than periodic rolls, the geometry of the caustics due to the deviation of the extraordinary rays can be very intricate [12]. Moreover, the caustics do not give in general a direct image of the director field, in the sense that the contrast cannot be expressed as an explicit function of the director field. We will now see that, on the contrary, in ordinary light and in thick layers, a contrast can be obtained which is easily interpretable for all types of weak distortions of the director field.

The propagation of the ordinary rays follows the Fermat principle now applied to the optical path associated with the index n_o. Since n_o is only function of the local temperature, and $dn_o/dT > 0$, one expects the rays to be focused above the warm flows, and defocused above the cold flows; ultimately a caustic should be formed, but only far away from the cell, since the temperature-induced index variations are very small. Experimentally, we observe in transmitted ordinary light a weak contrast immediately above the cell. The corresponding intensity profiles, taken perpendicularly to a roll structure, present a period half of the one expected if the contrast were due to the temperature-induced index variations (Fig. 4). Thus intrinsically anisotropic effects totally overcome the effect of the temperature-induced variations of n_o In fact, we can even deduce from Figure 4 that a simple expression of the transmitted intensity would be:

$$I(\mathbf{r}) \simeq I_0 + I_1 \ \sin^2(\mathbf{q} \cdot \mathbf{r})$$

which coincides (compare the above equation and (5)) with:

$$I(\mathbf{r}) \simeq I_0 + I_1' \ \tilde{n}_z^2(\mathbf{r}).$$

We will now interpret and justify this contrast in $\tilde{n}_z^2$.

A first idea is to look for scattering effects, which are very important in nematic liquid crystals. In effect, the thermal fluctuations of the director orientation are only weakly damped in nematics, and may therefore induce a strong light-scattering [15]. It was shown for instance in [16] that a homeotropic ($\mathbf{n} = \hat{\mathbf{z}}$) layer scatters less than a planar ($\mathbf{n} = \hat{\mathbf{x}}$) layer when illuminated

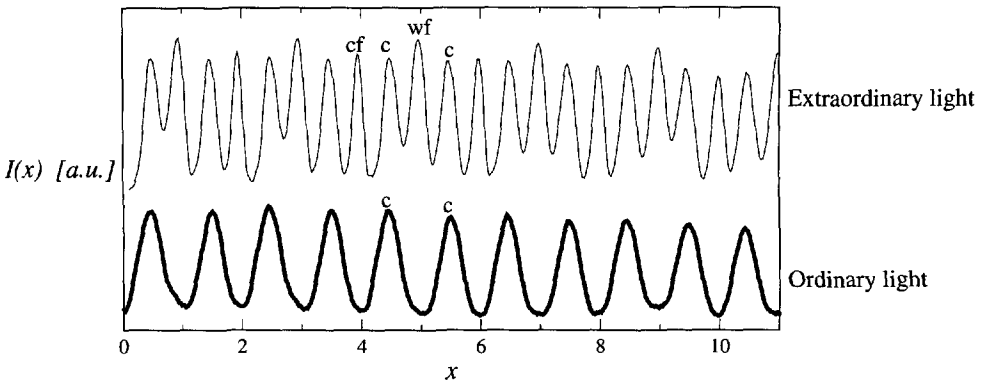

Fig. 4. — Typical intensity profiles obtained in transmitted polarized light, with a large depth of field ($\simeq$ 10 mm) objective focused above the top of the layer The position x in the horizontal plane is indicated in units of the layer thickness; the period of the convection rolls is 2. In extraordinary light (thin line), one observes not only the real cusps, *i.e.* the warm-flow (wf) and cold-flow (cf) cusps, but also the virtual cusps, associated with the centers (c) of the rolls. In ordinary light (thick line), the contrast is not interpretable in terms of the temperature-induced variations of the index, since warm and cold flows appear identically dark

in ordinary light: therefore the homeotropic layer transmits more light and appears brighter when observed from above. In our experiments, the director is raised in the centers of the rolls, *i.e.* close to the homeotropic geometry: the same scattering effects could then be responsible for the brighter aspect of the centers of the rolls. The authors of [16] investigated (both theoretically and experimentally) the special case of homogeneous nematic layers both in the planar and in the homeotropic geometry. We firstly propose hereafter a physical interpretation of the difference of transmitted intensity between the homeotropic and planar nematic layers We secondly calculate theoretically the transmission coefficients for a layer where the director is oblique ($\mathbf{n}$ homogeneous, but making a finite angle with $\hat{\mathbf{x}}$ and $\hat{\mathbf{z}}$), and then for a layer where the director is distorted We end by some applications to our experiments.

3.1. Interpretation of the Scattering Effects. — The scattering cross-section from an incident plane wave of wavevector $\mathbf{k}_i$ and of polarization $\mathbf{i}$ to an outgoing plane wave of wavevector $\mathbf{k}_f = \mathbf{k}_i + \mathbf{p}$ and of polarization $\mathbf{f}$ has been given for nematic liquid crystals in [16] ($\mathbf{i}$ and $\mathbf{f}$ are unit vectors). It should be valid in our case, assuming the hypothesis of *local equilibrium*: on a scale large as compared with the characteristic value of $2\pi/|\mathbf{p}| \simeq \lambda_0$ wavelength of the light, but small as compared with the macroscopic dimensions of the layer, the statistical average $\mathbf{n}_0$ of $\mathbf{n}$ can be considered as homogeneous, and the fluctuations $\delta\mathbf{n}$ of $\mathbf{n}$ as given by the equilibrium thermodynamics. Because of non-equilibrium effects, *i.e.* of the couplings with the other fields (which lead to the instability and create the distortion), a renormalization of these director fluctuations should only come into play for scattering wavevectors $\mathbf{p}$ close to the wavevector of the distortion [17]. But this corresponds to very small angle scattering (typically at $(\widehat{\mathbf{k}_i, \mathbf{k}_f}) \simeq \lambda_0/d \simeq 0\,6\ \mu$m/1 mm$\simeq$ 0.0006 rad) which we in fact include experimentally in the transmitted intensity. We therefore do not need to take into account these renormalization effects for the estimation of the intensity scattered at angles larger than $0.1° \simeq 0.002$ rad., and scattering wavevectors much larger than the distortion wavevector. Note also that the effects of small magnetic fields on the light scattering properties are negligible [16] To write down the

scattering cross-section formula, one uses an orthogonal basis $(\hat{\mathbf{e}}_1, \hat{\mathbf{e}}_2, \mathbf{n}_0)$ on which the director fluctuations are projected according to:

$$\mathbf{n} = \mathbf{n}_0 + \delta\mathbf{n} = \mathbf{n}_0 + \sum_{\alpha=1,2} n_\alpha \hat{\mathbf{e}}_\alpha .$$

The scattering cross-section is [16]:

$$\sigma_s(\mathbf{p}, \mathbf{f}) = \left(\epsilon_a \frac{\omega^2}{4\pi c^2}\right)^2 \frac{n_p(\theta_p)}{n_o \cos^2\delta} \frac{k_B T}{K\mathbf{p}^2} \sum_{\alpha=1,2} [(\mathbf{f}\cdot\mathbf{n}_0)(\hat{\mathbf{e}}_\alpha\cdot\mathbf{i}) + (\mathbf{f}\cdot\hat{\mathbf{e}}_\alpha)(\mathbf{n}_0\cdot\mathbf{i})]^2 \qquad (9)$$

in which one distinguishes three factors:

- the geometrical factor $(\epsilon_a\omega^2/(4\pi c^2))^2\, n_p(\theta_p)/(n_o\cos^2\delta)$, where $\epsilon_a = n_e^2 - n_o^2$ is the dielectric anisotropy, ω the frequency and c the velocity of light in vacuum. The angles $\theta_p = (\widehat{\mathbf{n}, \mathbf{k}_f})$ and δ are associated with the scattered wave and differ from zero only in the case of an extraordinarily scattered light wave. This factor presents small variations (of order 10% at most) as a function of the scattering geometry, since n_p (3) is always of the order of n_o, and δ (4) is always small.

- the thermodynamic-energetic factor $k_B T/K\mathbf{p}^2$, which is the amplitude of the director fluctuations of wavevector $\mathbf{p}$. There k_B is the Boltzmann's constant, and $K\mathbf{p}^2$ the energetic cost of this modulation, K beeing an average of the splay, twist and bend elastic constants (we use the one elastic constant approximation in order to simplify the calculations). The divergence of this factor for small $\mathbf{p}$ means that the long-wavelength fluctuations are of course the strongest ones, and implies that the scattering can only be important *at small angles* $(\widehat{\mathbf{k}_i, \mathbf{k}_f})$.

- the polarization factor $\sum_{\alpha=1,2}[...]$, which can be shown to result directly from the projection of the "director-radiated" dipolar field on the final polarization $\mathbf{f}$ [15]. This factor depends strongly of the scattering geometry, since it can cancel for some of these geometries.

As a consequence, the *values of the polarization factor at small angles* will control the value of $\sigma_s(\mathbf{p}, \mathbf{f})$.

We now consider our two limit cases of either a planar (director horizontal $\mathbf{n}_0 = \hat{\mathbf{x}}$), or a homeotropic (director vertical $\mathbf{n}_0 = \hat{\mathbf{z}}$) nematic layer, illuminated from below in ordinary light: $\mathbf{k}_i = \hat{\mathbf{z}}$ and $\mathbf{i} = \hat{\mathbf{y}}$. Thus $\mathbf{n}_0 \cdot \mathbf{i}$ vanishes, and this reduces the polarization factor to:

$$(\mathbf{f}\cdot\mathbf{n}_0)^2 \sum_{\alpha=1,2} (\hat{\mathbf{e}}_\alpha\cdot\mathbf{i})^2 = (\mathbf{f}\cdot\mathbf{n}_0)^2 \qquad (10)$$

since $\mathbf{i}$ belongs to the plane $(\hat{\mathbf{e}}_1, \hat{\mathbf{e}}_2)$. This implies that the scattering will occur in extraordinary light (if both $\mathbf{i}$ and $\mathbf{f}$ are perpendicular to $\mathbf{n}_0$, *i e.* if the electric field is supposed to be always perpendicular to the director, it is clear, from the symmetries of the nematic phase, that no anisotropic scattering effect can occur). At small scattering angles, since $\mathbf{k}_i = \hat{\mathbf{z}}$, one has also $\mathbf{k}_f \simeq \hat{\mathbf{z}}$. We deduce therefore from the fact that $\mathbf{f}$, $\mathbf{k}$ and $\mathbf{P}$ are coplanar, and from the smallness of the angle δ given by (4) (since n_o^2/n_e^2 is always larger than 0.75, one has, $\forall\,\theta_p$ in $[0, \pi/2]$, $\delta < 0.15$ rad), that:

$$(\widehat{\mathbf{f}, \hat{\mathbf{z}}}) \simeq (\widehat{\mathbf{f}, \mathbf{k}_f}) = (\widehat{\mathbf{f}, \mathbf{P}}) + (\widehat{\mathbf{P}, \mathbf{k}_f}) = \frac{\pi}{2} + \delta \simeq \frac{\pi}{2}$$

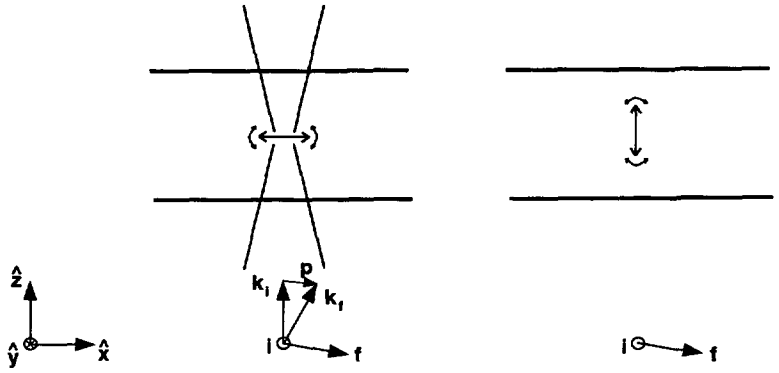

Fig. 5. — Sketches indicating the physical origin of the difference of transmission of ordinary light between a planar (left) and a homeotropic (right) nematic layer. In both cases the light scattering may be induced by the long-wavelength fluctuations (of small wavevector $\mathbf{p}$) of the director orientation, *i.e.* at small angles $(\widehat{\mathbf{k}_i, \mathbf{k}_f})$ between the wavevector of the incoming ordinary light and the scattered extraordinary light. For the latter, the polarization $\mathbf{f}$ stays roughly horizontal, and therefore in the homeotropic geometry (right) no coupling of the electric field with the director can occur. Consequently there is no scattering and the intensity of the transmitted ordinary light is higher, as compared with the planar layer.

Hence at small scattering angles, $\mathbf{f}$ stays roughly perpendicular to $\mathbf{k}_f$ (like in light waves in isotropic media), *i.e.* roughly horizontal. In consequence, in the homeotropic layer, $\mathbf{f}$ has only a very small projection on $\mathbf{n}_0 = \hat{\mathbf{z}}$, and the scattering intensity is very weak. On the contrary, in the planar layer, the polarization factor $(\mathbf{f} \cdot \mathbf{n}_0)^2$ can reach its highest possible value of 1, and the scattering intensity is strong. These effects, sketched in Figure 5, explain why in the homeotropic layer the ordinary light is almost completely transmitted, contrary to the planar case.

In the more general case of a oblique director:

$$\mathbf{n}_0 = \hat{\mathbf{x}} \cos\phi + \hat{\mathbf{z}} \sin\phi \tag{11}$$

the highest value of the polarization factor at small angles will be reached for $\mathbf{f} = \hat{\mathbf{x}}$, and read:

$$(\mathbf{f} \cdot \mathbf{n}_0)^2 \simeq (\hat{\mathbf{x}} \cdot \mathbf{n}_0)^2 \simeq \cos^2\phi \simeq 1 - \phi^2.$$

Since this polarization factor controls the values of the total scattering cross-section, we can estimate that it will take a form in $a - b\phi^2$, and therefore that the transmitted intensity will be $a' + b'\phi^2$ as it could be deduced experimentally.

3.2. Calculation of the transmission coefficients. — We first consider the case of a oblique layer, where the director is homogeneously tilted as expressed by (11). The incident ordinary light wave propagates vertically in the layer. In consequence, the polarization factor simplifies according to (10), and the scattering can only occur in extraordinary light. All geometry-dependent factors in (9) can then be expressed as a function of the new variable $u = \cos\theta_p$. We also introduce $b = n_e/n_o$ as in [16]. The outlines of these trigonometric calculations are the followings:

- for the polarization factor, since:

$$(\widehat{\mathbf{f}, \mathbf{n}_0}) = (\widehat{\mathbf{f}, \mathbf{P}}) + (\widehat{\mathbf{P}, \mathbf{n}_0}) = \pi/2 + \theta_r$$

it reads simply:

$$(\mathbf{f} \cdot \mathbf{n}_0)^2 = \sin^2 \theta_r$$

and it can be expressed as a function of $\tan^2 \theta_r$, and then of $\tan^2 \theta_p$ and u^2 according to the relation:

$$\tan \theta_r = b^{-2} \tan \theta_p$$

- the phase index is:

$$\frac{n_p(\theta_p)}{n_o} = b\,[1 + (b^2 - 1)u^2]^{-1/2} = n_p(u)$$

- the $\cos^{-2} \delta = 1 + \tan^2 \delta$ factor can also be expressed as a function of $\tan \theta_p$ and u with the relation (4).

Finally, one obtains·

$$(\mathbf{f} \quad \mathbf{n}_0)^2 \frac{n_p(\theta_p)}{n_o \cos^2 \delta} = b^{-4}\, n_p^5(u)\,(1 - u^2)$$

To compute the energetic factor $\mathbf{p}^{-2} = (\mathbf{k}_f - \mathbf{k}_i)^{-2}$, we need to specify the coordinates of the wavevectors. We scale them in units of the wavevector of the incident ordinary light $|\mathbf{k}_i| = n_o \frac{\omega}{c}$. According to (11), we can choose a basis $(\hat{\mathbf{e}}_1, \hat{\mathbf{e}}_2, \mathbf{n}_0)$ such that:

$$\mathbf{k}_i = \hat{\mathbf{z}} = \hat{\mathbf{e}}_2 \cos \phi + \mathbf{n}_0 \sin \phi \tag{12}$$

In this basis, $\mathbf{k}_f$, of dimensionless norm equal to $n_p(u)$, is expressed in spherical coordinates (θ_p, φ) according to:

$$\mathbf{k}_f = n_p(u)\,(\hat{\mathbf{e}}_1 \sin \theta_p \cos \varphi + \hat{\mathbf{e}}_2 \sin \theta_p \sin \varphi + \mathbf{n}_0 \cos \theta_p).$$

We then obtain:

$$\mathbf{p}^2 = (\mathbf{k}_f - \mathbf{k}_i)^2 = 1 + n_p^2(u) - 2\, n_p(u)\,(\cos \theta_p \sin \phi + \sin \theta_p \cos \phi \sin \varphi)$$

In the total local scattering cross-section, which will be a function of the angle of the director ϕ only:

$$\sigma_s(\phi) = \int_{\varphi=0}^{2\pi} \int_{\theta_p=0}^{\pi} \mathrm{d}\varphi\, \sin \theta_p\, \mathrm{d}\theta_p\, \sigma_s(\mathbf{p}, \mathbf{f})$$

the integration on φ can be calculated analytically. We obtain, as a function of $n_z = \sin \phi$ instead of ϕ:

$$\begin{aligned} I_\varphi(u; n_z) &= \int_{\varphi=0}^{2\pi} \frac{\mathrm{d}\varphi}{\mathbf{p}^2} \\ &= 2\pi\, [\, (1 - n_p^2(u))^2 - 4\, n_p(u)\,(1 + n_p^2(u))\, u\, n_z + 4\, n_p^2(u)\,(n_z^2 + u^2)\,]^{-1/2} \end{aligned}$$

where the scaling factor on $\mathbf{p}^{-2}$ has been taken out Finally:

$$\sigma_s(n_z) = \frac{k_B T}{16\pi^2} \left(\frac{\omega}{c}\right)^2 \frac{\epsilon_a^2}{K n_o^2 b^4} \int_{u=-1}^{1} \mathrm{d}u\,(1 - u^2)\, n_p^5(u)\, I_\varphi(u; n_z). \tag{13}$$

The last integral can only be numerically computed.
The prefactor is, in the case of 5 CB at 28 °C ($K = 5.59$ pN [18,19]), with the optical indices given in Section 2.1·

$$\frac{k_B T}{16\pi^2} \left(\frac{2\pi}{\lambda_0}\right)^2 \frac{\epsilon_a^2}{K n_o^2 b^4} = \frac{k_B T}{4K} \left(\frac{n_o}{\lambda_0}\right)^2 (1 - b^{-2})^2 = 33 \text{ m}^{-1}.$$

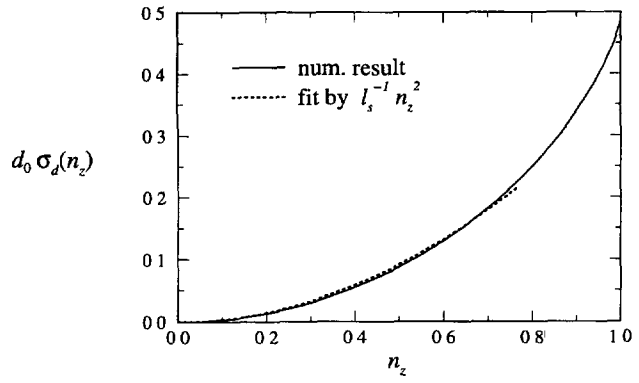

Fig. 6 — Rescaled variation of the scattering cross-section between planar ($n_z = 0$) and oblique ($n_z \neq 0$) geometries $\sigma_d(n_z) = \sigma_s(0) - \sigma_s(n_z)$ The scale factor $d_0 = 1$ mm has been taken as a typical layer thickness (see text) The scattering cross-section $\sigma_s(n_z)$ decreases when one approaches the homeotropic geometry $n_z = 1$

Figure 6 presents our results on $\sigma_s(n_z)$; since $\sigma_s(n_z)$ indeed decreases when n_z increases, we rather plotted $\sigma_d(n_z)$ defined by:

$$\sigma_s(n_z) = \sigma_s(0) - \sigma_d(n_z) \tag{14}$$

It is very well approximated, for $|n_z| = |\sin\phi| < 0.77$, *i.e.* $|\phi| < 50^o$, by:

$$\sigma_d(n_z) = l_s^{-1} n_z^2 \tag{15}$$

where the characteristic length is found to be:

$$l_s = 2\ 7 \text{ mm}$$

Let us now consider the case of a layer where the director field is weakly distorted along the z direction. We introduce the angle $\phi(z) = \arcsin n_z(z)$ between the horizontal plane and the director, and assume oblique anchoring boundary conditions: $\mathbf{n}$ given by (11) at the boundaries, with $\phi = \phi(0) < 90^o$ (note that $\phi(0) = 0$ corresponds to the planar anchoring). We assume that the director never gets vertical, so that the generalized principle of Mauguin [20] is valid. It expresses that the incident ordinary light wave will propagate vertically, its polarization $\mathbf{i}$ rotating so as to stay perpendicular to the plane $(\hat{\mathbf{z}}, \mathbf{n}) = (\mathbf{k}_i, \mathbf{n})$. Locally the scattering geometry will therefore be identical to the one used in the previous calculations, but possibly rotated if there exists a smooth n_y component The incident ordinary light wave still arrives with $\mathbf{k}_i = |\mathbf{k}_i|\hat{\mathbf{z}}$, and the director still makes an angle of $\pi/2 - \phi(z)$ with $\mathbf{k}_i$. Thus a basis $(\hat{\mathbf{e}}_1, \hat{\mathbf{e}}_2, \mathbf{n}_0)$ which satisfies (12), with $\phi = \phi(z)$, can still be chosen, and all our local calculations are valid. The loss of ordinary light intensity by the scattering in the elementary layer $[z, z+\mathrm{d}z]$ being:

$$\frac{\mathrm{d}I}{\mathrm{d}z} = -\sigma_s(n_z(z))\, I(z)$$

we obtain for the transmission coefficient:

$$\tau = \frac{I_{transmitted}}{I_{incident}} = \frac{I(d)}{I(0)} = \exp\Big(- d \int_{z=0}^{1} \sigma_s(n_z(z))\mathrm{d}z \Big)$$

where, in the integral, our z coordinates are still scaled in units of the layer thickness d. With (14), defining $\tau_0 = \exp(-d\,\sigma_s(0))$, which does not depend of the director field in the layer, we get:

$$\tau = \tau_0 \ \exp\Big(d \int_{z=0}^{1} \sigma_d(n_z(z))\mathrm{d}z\Big). \tag{16}$$

For a homogeneous layer we have:

$$\ln\tau = \ln\tau_0 + d\,\sigma_d(n_z).$$

This gives a simple physical meaning to the curve plotted in Figure 6: $d_0\ \sigma_d(n_z)$, with $d_0 = 1$ mm, is the difference of the logarithms of the intensities transmitted on one hand by a oblique layer of thickness 1 mm (inside which $n_z \neq 0$) and on the other hand by a planar layer of thickness 1 mm (inside which $n_z = 0$).

Now, in the case of a layer where the director component n_z is in addition modulated as a function of the position $\mathbf{r}$ in the horizontal plane, the previous calculations apply locally. We come back for simplicity reasons to the planar case, and assume sine vertical profiles, *cf.* (1). If in (1) $|\tilde{n}_z(\mathbf{r})|$ stays smaller than 0.77, we can use the expansion (15) of $\sigma_d(n_z)$, and perform the vertical integration in (16). This gives:

$$\frac{\tau(\mathbf{r})}{\tau_0} = \exp\Big(\frac{d}{2l_s}\tilde{n}_z^2(\mathbf{r})\Big) = 1 + \frac{d}{2l_s}\,\tilde{n}_z^2(\mathbf{r}) + \text{h.o.t.} \tag{17}$$

For small distortions, we have:

$$\frac{d}{2l_s}\,\tilde{n}_z^2(\mathbf{r}) < \frac{d}{2l_s}0.77^2 = \frac{d}{9\ 1\text{mm}}.$$

This result proves that for all our thermoconvective cells, of maximal thickness 1.5 mm, the higher order terms in (17) can indeed be neglected, and the law in $\tilde{n}_z^2(\mathbf{r})$ deduced from the experiments is valid. Moreover, this explains why these scattering effects have not been observed in the electroconvective experiments, where the cells are of maximum thickness of order 100 μm (for which $d/9.1$ mm=0.01$\ll$1).

The consequence of the Mauguin principle, that the final contrast is independent of n_y, is confirmed by our experimental observations on oblique roll structures, where nonzero n_y components exist [7]. Indeed, the intensity profiles (taken perpendicularly to the rolls) in transmitted ordinary light are on oblique rolls identical to the ones observed on normal rolls (as in Fig. 4).

We note finally that, in the case of a layer with a oblique undirectional anchoring, where the n_z distortion takes the form $n_z(\mathbf{r}, z) = \bar{n}_z + \tilde{n}_z(\mathbf{r})\sin(\pi z)$, a contrast linear in $\tilde{n}_z(\mathbf{r})$ is then expected from (16), (15).

3.3. APPLICATIONS. — We apply this method to characterize accurately a more complex structure. This structure is the varicose, which was obtained for the first time in thermoconvection in our experiments [5]. This structure had been first obtained in electroconvection [21]. We will now show that it can be reconstructed in good approximation as the superposition of two roll structures. This implies that the $\tilde{n}_z(\mathbf{r})$ field can be written, at leading order, as:

$$\tilde{n}_z(\mathbf{r}) = A\sin(\mathbf{q}\ \ \mathbf{r}) + B\sin(\mathbf{k}\ \ \mathbf{r}). \tag{18}$$

Here $\mathbf{q}$ is the wavevector of the primary oblique roll structure and $\mathbf{k}$ is a secondary wavevector, since this structure appears as the result of a secondary instability of the oblique roll $\mathbf{q}$ structure

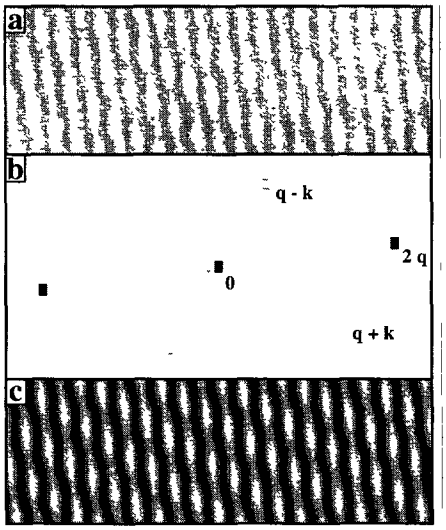

Fig. 7 — a) typical varicose structure, obtained in the thermoconvection of 5CB, and imaged in ordinary polarized light. b) numerical structure factor (square of the modulus of the Fourier transform) of the above image The peaks positions and intensity are compatible with the ansatz (19), and lead to the determination of the wavectors **q**, **k**, and of the ratio B/A (between the amplitudes of the two modes, see text) c) numerical image reconstructed in direct space with the bimodal model (18), (19).

[5,21]. We test the validity of (18) by imaging the structure in ordinary light, as in Figure 7a, where we should observe according to (17), (18) a variation of intensity given by:

$$I(\mathbf{r}) \propto \tilde{n}_z^2(\mathbf{r}) = \frac{A^2}{2}[1-\cos(2\mathbf{q}\cdot\mathbf{r})]+AB[\cos((\mathbf{q}-\mathbf{k})\cdot\mathbf{r})-\cos((\mathbf{q}+\mathbf{k})\cdot\mathbf{r})]+\frac{B^2}{2}[1-\cos(2\mathbf{k}\cdot\mathbf{r})]. \quad (19)$$

This means that the Fourier spectrum of our images must present only four main peaks centered around $2\mathbf{q}, \mathbf{q}\pm\mathbf{k}$ and $2\mathbf{k}$, with the following powers (in arbitrary units):

$$|\hat{I}(2\mathbf{q})| = \frac{A^2}{2}, \quad |\hat{I}(\mathbf{q}+\mathbf{k})| = |\hat{I}(\mathbf{q}-\mathbf{k})| = AB, \quad |\hat{I}(2\mathbf{k})| = \frac{B^2}{2}. \quad (20)$$

Our varicose images, such that the one shown in Figure 7a, are digitized on a 512×512 pixel grid in 256 gray levels, and their Fast Fourier Transform is then computed. We show in Figure 7b the deduced structure factor $S = |\hat{I}|^2$. It comprises three main peaks centered around $2\mathbf{q}$ and $\mathbf{q}\pm\mathbf{k}$, for which we obtain by integration on a few pixels around each peak:

$$|\hat{I}(2\mathbf{q})| = 0.371, \quad |\hat{I}(\mathbf{q}+\mathbf{k})| = 0.109, \quad |\hat{I}(\mathbf{q}-\mathbf{k})| = 0.128$$

We have not shown the peak at $2\mathbf{k}$ which is very weak. This result agrees with (20), except for the small difference between $|\hat{I}(\mathbf{q}+\mathbf{k})|$ and $|\hat{I}(\mathbf{q}-\mathbf{k})|$ which may be due to experimental or intrinsic inhomogeneities. The positions of the peaks allow one to determine the wavevectors $\mathbf{q}$ and $\mathbf{k}$. Moreover, according to (20), and taking into account the fact that we do not measure exactly the same values for $|\hat{I}(\mathbf{q}+\mathbf{k})|$ and $|\hat{I}(\mathbf{q}-\mathbf{k})|$, we can derive a *method of measurement* of the ratio B/A from:

$$\frac{B}{A} = \frac{1}{4}\frac{|\hat{I}(\mathbf{q}+\mathbf{k})|+|\hat{I}(\mathbf{q}-\mathbf{k})|}{|\hat{I}(2\mathbf{q})|}. \quad (21)$$

This gives here $B/A = 0.16$, from which we get using (20), $S(2\mathbf{k})/S(2\mathbf{q}) = (B/A)^4 \ll 1$, and thus one understands why the peak at $2\mathbf{k}$ was nearly invisible on the structure factor. We finally prove the validity of our model (18) by computing, from the values of $\mathbf{q}$, $\mathbf{k}$ and B/A deduced from the Fourier transform of the image, the numerical image predicted for $I(\mathbf{r})$ (19). We find a very good agreement between the experimental image Figure 7a and our simulation Figure 7c.

4. Conclusion

We have developped in this article new optical methods for the characterization of distorted nematic layers with planar anchoring boundary conditions. Our methods, which use transmitted polarized light, allow rather directly a full characterization of the distortion of the vertical component n_z of the director.

In extraordinary polarized light, we have proposed a new geometrical measurement of the director distortion by measuring the angle of aperture of the cusps, *i.e.* maximal deflection angles. This measurement is easy to perform, and does not depend on the precise experimental setup (by contrast with the classical measurement of the height of the cusp points). It leads, through simple nonlinear relations, to the amplitude of the distortion, as we have shown for structures of convective rolls. It is well adapted for the measurement of not too small amplitudes. An extension of this method of measurement to the bimodal structures is under study. This method could of course be generalized to other systems producing caustics, such as isotropic thermoconvection.

In ordinary polarized light, we have calculated a new type of contrast, explained by director-induced scattering effects. This contrast gives the map of $n_z^2(\mathbf{r})$, assuming the simplest vertical profile compatible with the boundary conditions, but for any horizontal variations of the director. It is, to our knowledge, the first method in experimental nematodynamics which permits to see directly a director component. It could of course, be used in other experiments, as soon as the nematic layer is thick enough ($d \gtrsim 1$ mm) to permit the observation of scattering effects.

The values of the coefficients used in our calculations for other liquid crystals than 5CB are avalaible from the authors upon request.

Acknowledgments

This work was supported by the Direction des Recherches et Études Techniques under contract DGA/DRET/94136.

References

[1] Merzkirch W , Flow Visualization (Academic Press, Orlando, 1987).
[2] For a recent review, see Buka A. and Kramer L., Pattern formation in liquid crystals (Springer-Verlag, New-York, 1996).
[3] Rasenat S., Hartung G., Winkler B.L. and Rehberg I., *Exp. Fluids* **7** (1989) 412.
[4] Dubois-Violette E., Guyon E. and Pieranski P., *Mol. Cryst. Liq. Cryst.* **26** (1974) 193.
[5] Plaut E. and Ribotta R., *Europhys. Lett.* **38** (1997) 441.
[6] Feng Q., Pesch W. and Kramer L., *Phys. Rev. A* **45** (1992) 7242.
[7] Plaut E. and Ribotta R., *Phys. Rev. E* **56** (1997) R2375.

[8] Born M. and Wolf E., Principles of optics (Pergamon Press. 1980).
[9] Joets A. and Ribotta R., *Optics Comm.* **107** (1994) 200.
[10] Sushmita S., Brahma P., Roy S. K., Mukherjee D. K. and Roy S. B., *Mol. Cryst. Liq. Cryst.* **100** (1983) 327.
[11] Kline M. and Kay I., Electromagnetic theory and geometrical optics (Interscience Publishers, 1965).
[12] See for instance the description of the caustics produced by the "varicose" distortion in Joets A. and Ribotta R., *Phys. Rev. Lett.* **77** (1996) 1755.
[13] Joets A. and Ribotta R., *J. Phys. I France* **4** (1994) 1013.
[14] Joets A. and Ribotta R., in preparation.
[15] de Gennes P. G., The Physics of Liquid Crystals (Clarendon Press, Oxford, 1974).
[16] Langevin D. and Bouchiat M.A., *J. Phys. France* **36** (1975) C1-197.
[17] See for instance Treiber M. in [2], and references therein.
[18] Bradshaw M. J., Raynes E. P., Bunning J. D. and Faber T. E., *J. Phys. France* **46** (1985) 1513.
[19] Coles H J. and Sefton M. S., *Molec. Cryst. Liq. Cryst. Let.* **1** (1985) 151.
[20] C. Mauguin, *Bull. Soc. Fr. Min.* **34** (1911) 71
[21] Ribotta R. and Joets A., *J. Phys. France* **47** (1986) 739